Received: 8 February 2019 | Revised: 12 March 2019 | Accepted: 26 March 2019

DOI: 10.1111/jace.16467

ORIGINAL ARTICLE

Journal of the American Ceramic Society

Effect of particle size distribution of metakaolin on hydration kinetics of tricalcium silicate

Jonathan Lapeyre[1] | **Hongyan Ma**[2] | **Aditya Kumar**[1]

[1]Department of Materials Science and Engineering, Missouri University of Science and Technology (S&T), Rolla, Missouri

[2]Department of Civil, Architectural, and Environmental Engineering, Missouri University of Science and Technology (S&T), Rolla, Missouri

Correspondence
Aditya Kumar, Department of Materials Science & Engineering, Missouri University of Science and Technology, Rolla, MO.
Email: kumarad@mst.edu

Funding information
Division of Civil, Mechanical and Manufacturing Innovation, Grant/Award Number: 1661609 and 1761697

Abstract

The focus of this study is to elucidate the role of particle size distribution (PSD) of metakaolin (MK) on hydration kinetics of tricalcium silicate (C_3S–T_1) pastes. Investigations were carried out utilizing both physical experiments and phase boundary nucleation and growth (pBNG) simulations. [C_3S + MK] pastes, prepared using $8\%_{mass}$ or $30\%_{mass}$ MK, were investigated. Three different PSDs of MK were used: fine MK, with particulate sizes <20 μm; intermediate MK, with particulate sizes between 20 and 32 μm; and coarse MK, with particulate sizes >32 μm. Results show that the correlation between specific surface area (SSA) of MK's particulates and the consequent alteration in hydration behavior of C_3S in first 72 hours is nonlinear and nonmonotonic. At low replacement of C_3S (ie, at $8\%_{mass}$), fine MK, and, to some extent, coarse MK act as fillers, and facilitate additional nucleation and growth of calcium silicate hydrate (C–S–H). When C_3S replacement increases to $30\%_{mass}$, the filler effects of both fine and coarse MK are reversed, leading to suppression of C–S–H nucleation and growth. Such reversal of filler effect is also observed in the case of intermediate MK; but unlike the other PSDs, the intermediate MK shows reversal at both low and high replacement levels. This is due to the ability of intermediate MK to dissolve rapidly—with faster kinetics compared to both coarse and fine MK—which results in faster release of aluminate [$Al(OH)_4^-$] ions in the solution. The aluminate ions adsorb onto C_3S and MK particulates and suppress C_3S hydration by blocking C_3S dissolution sites and C–S–H nucleation sites on the substrates' surfaces and suppressing the post-nucleation growth of C–S–H. Overall, the results suggest that grinding-based enhancement in SSA of MK particulates does not necessarily enhance early-age hydration of C_3S.

KEYWORDS

filler effect, hydration kinetics, metakaolin, particle size, tricalcium silicate (C_3S)

1 | INTRODUCTION

The benefits of partially replacing ordinary portland cement (subsequently referred to as cement) with widely available and abundant aluminosilicate materials (eg, waste glass, calcined clays, blast furnace slag, and fly ash) have been widely investigated as part of a broad strategy to offset the environmental effects (ie, CO_2 emissions and energy consumption) of cement production.[1–6] When cement or tricalcium silicate (C_3S: the major phase in cement) is partially

replaced with an aluminosilicate material (ie, [cement/C_3S + aluminosilicate] pastes), hydration kinetics of the former are altered on account of two effects exerted by the additive, that is, filler effect and pozzolanic effect.[7–9] Both effects enhance formation of calcium silicate hydrate (C–S–H[1]: the major hydration product in cement and C_3S systems), albeit through two different processes. The filler effect is a physical mechanism, wherein fine particles of the additive act as energetically favorable substrates for heterogeneous nucleation and subsequent growth of C–S–H nuclei.[8–12] The additional C–S–H formed as a result of the filler effect results in improved solid-to-solid phase connectivity within the microstructure, thus leading to improved properties (eg, compressive strength) of the bulk material.[8,10,13] Although fillers are typically assumed to be inert, aluminosilicate, as well as silica based (eg, silica fume), material additives are also able to undergo pozzolanic reaction in cementitious environments.[9,14–18] The pozzolanic reaction pertains to chemical reaction of the aluminosilicate/silicate additive with portlandite (CH or calcium hydroxide) to produce C–S–H.[19–23] The additional (pozzolanic) C–S–H formed as a result of the pozzolanic reaction is a space-filling hydrate (especially when compared to its precursor, CH) and contributes toward enhancement of the bulk material's physical properties, such as lowering water permeability and improving strength.[24–28]

The focus of this study is metakaolin ($Al_2Si_2O_7$: subsequently abbreviated as MK), an anhydrous aluminosilicate material derived from calcination of kaolinite ($Al_2Si_2O_5(OH)_4$) clay at temperatures between 500°C and 800°C.[29–32] Calcination of kaolin above 900°C transforms MK into crystalline mullite and/or γ-Al_2O_3, significantly attenuating its pozzolanic reactivity.[31–33] Calcination breaks covalent bonds between hydroxyl groups and aluminum octahedral groups transforming the triclinic crystal structure of kaolinite into an amorphous network.[34,35] The amorphous structure is energetically less stable than the crystalline structure, thus leading to faster dissolution dynamics and enhanced overall reactivity of MK, as compared to kaolin, in alkaline conditions of cement and C_3S pastes.[21,36–38]

There have been several investigations identifying and assessing the benefits of MK, as well as other calcined clay minerals, when used to replace cement in pastes, concretes, and mortars.[21–23,39–41] While majority of these studies have focused on quantifying the aforementioned benefits in terms of improvement in properties of the bulk material,[31,42] there are only a few studies that have examined, and attempted to decouple, the filler and pozzolanic contributions of MK. Notable among these is a recent study conducted by Lapeyre and Kumar,[9] in which hydration behavior of C_3S in [C_3S + MK] pastes were examined. The study concluded that the pozzolanic activity of MK is negligible at early ages (ie, up to 24 hours after mixing), and, therefore, does not cause significant alteration in hydration behavior of C_3S. MK, however, does serve as a filler, and facilitates nucleation and growth of C–S–H on its particulates' surface. At low replacements (ie, up to 10% $_{mass}$) of C_3S, the filler effect of MK is substantial, and even superior in comparison to that of silica fume, the fine particulates of which are highly susceptible to effects of particle agglomeration. At higher replacement levels (ie, ≥20%), however, the filler effect of MK is either substantially diminished or reversed (ie, suppression, rather than enhancement, of C–S–H nucleation and growth). Such diminishment or reversal of MK's filler effect is attributed to the abundance of aluminate anions [$Al(OH)_4^-$] in the solution, released from the dissolution of MK. More specifically, the study[9] reported that the aluminate anions adsorb onto C_3S and MK particulates' surfaces, and inhibit topographical sites for C–S–H nucleation; furthermore, the same anions adsorb onto C–S–H and impede its post-nucleation growth. Such inhibition of C_3S hydration has also been reported in other aluminate-rich systems, for example, when Al_2O_3-doped C_3S (instead of pure C_3S) is used or when C_3S/cement pastes are provisioned with Al_2O_3 nanoparticles and highly soluble aluminate salts (eg, $NaAlO_2$ and $AlCl_3$).[43–47]

Based on the above discussion, it is apparent that dissolution dynamics of MK play a significant role in altering the hydration behavior of cementitious systems. It could be argued that any factor that affects MK's dissolution would also affect overall hydration of the host cementitious material. One such factor is the particle size distribution (PSD) of MK. This is based on a vast number of prior studies that have shown that in aqueous environments, finer particulates dissolve faster compared to coarser ones.[48–52] Prior literature, however, provides little information on the effect of PSD of MK on hydration kinetics of C_3S or cement systems. In two separate studies, conducted by Justice and Kurtis and Lagier and Kurtis[53,54] it was shown that fine MK particulates (90% of particulates finer than 2 μm) accelerated—albeit only slightly—the hydration of cement. However, in pastes prepared with MK comprised of particulates coarser than the aforementioned one, the filler effect was negligible; furthermore, the onset of acceleration period (ie, when massive precipitation of C–S–H and CH occur) in such pastes was significantly delayed. While insights provided by the aforementioned pair of studies[53,54] are significant, the utilization of cement—which is a multicomponent material, consisting of other phases (eg, C_3A) in addition to C_3S—makes it difficult to conclude that the effects of MK scale monotonically with fineness (ie, SSA: specific surface area) of its particulates. This is because in cement paste, the aluminate ions released from dissolution of MK can undergo reactions with paste components other

[1]Portions of the manuscript will implement standard cement chemistry notation: C = CaO, S = SiO_2, A = Al_2O_3, H = H_2, $ = SO_3.

than C_3S, resulting in precipitation of secondary hydrates (eg, strätlingite and hydrogarnet) and alterations in stability of sulfate-bearing phases (eg, ettringite).[1,21] Such reactions, and their net effect on cement's hydration behavior, make it difficult to sequester the filler and pozzolanic effects of MK from its overall effect. Thus, it is important to evaluate such behaviors in single-compound systems (eg, C_3S) that still feature the filler and pozzolanic effects, but present fewer complexities compared to cement.

This study investigates the influence of PSD of MK on its pozzolanic and filler effects in [C_3S + MK] pastes. Pastes featuring three different PSDs of MK and two different C_3S mass replacement levels (ie, $8\%_{mass}$ and $30\%_{mass}$) have been used. Toward the examination of hydration behavior of C_3S in such pastes, a combination of experimental methods (eg, isothermal microcalorimetry and TGA: thermogravimetric analysis) and phase boundary nucleation and growth (pBNG) simulations have been implemented. Emphasis has been given to consolidate results obtained from experiments and simulations to elucidate, from a mechanistic standpoint, the correlation between SSA of MK particulates and the resultant effect on C_3S hydration behavior in [C_3S + MK] pastes.

2 | MATERIALS AND METHODS

Triclinic C_3S (Ca_3SiO_5–T_1) was produced via solid-state thermal processing of reagent grade quartz and calcite precursors. Details regarding synthesis are presented elsewhere.[9] After synthesis, the final powder was evaluated—using x-ray diffraction and Rietveld analyses—to be nearly phase pure C_3S, containing only 0.80% ± 0.25% of residual free lime (ie, CaO). The composition of MK (Imerys-Kaolin Metastar HP501), in terms of mass percentages of oxides as determined from x-ray florescence, is shown in Table 1. As shown in the table, the MK powder is composed of $51.30\%_{mass}$ SiO_2 and $47.80\%_{mass}$ Al_2O_3, with minor titanium and iron oxide contaminants.

TABLE 1 Composition of metakaolin, in terms of oxides, as determined from x-ray fluorescence

Components	MK
#	$\%_{mass}$
SiO_2	51.30
Al_2O_3	47.80
Fe_2O_3	0.44
CaO	0.04
MgO	0.09
SO_3	<0.01
TiO_2	0.90
Na_2O equivalent	0.21
Loss of Ignition (LOI)	0.52

Three different particle sizes distributions (PSDs) of MK were generated from the bulk powder, utilizing a modified wet-sieving process based on the ASTM C325-07(2014)[55] method. It is clarified that both dry- and wet-sieving methods were attempted in this study; however, the latter was chosen as it resulted in superior particulate yields (ie, greater amounts) and better size classification of particulates into three unique PSDs as compared to the former method. With respect to the aforementioned ASTM standard, minor modifications in the wet-sieving method were made to ensure consistency between different batches of each PSD of MK. Notably, the amount of distilled water (used for mixing with MK to produce a wet mix) was set at ≈200 mL, and the mixture was shaken by hand to ensure homogeneity after the 2-hour shaking process. Although MK is the dehydrated form of kaolin, prior studies and results obtained from XRD (not shown), have shown that under standard temperature and pressure (STP) conditions, MK does not significantly rehydrate (during the wet-sieving process), and, therefore, does not revert back to kaolin.[56] As the final part of the wet-sieving process, the "as-received" PSD of MK was sifted through 20 μm and 32 μm sieves to yield three unique PSDs: (a) fine—with particulate sizes (ie, diameters) <20 μm; (b) intermediate—with particulate sizes ranging between 20 and 32 μm; and (c) coarse—with particulate sizes >32 μm. In the subsequent sections, the three PSDs of MK with increasing fineness are referred to as fine MK, intermediate MK, and coarse MK, respectively. All PSDs of MK, as well as of C_3S, were measured using a static light scattering (SLS) analyzer (Microtrac S3500). Toward this, the powders were suspended in isopropanol, and agitated with ultrasonic

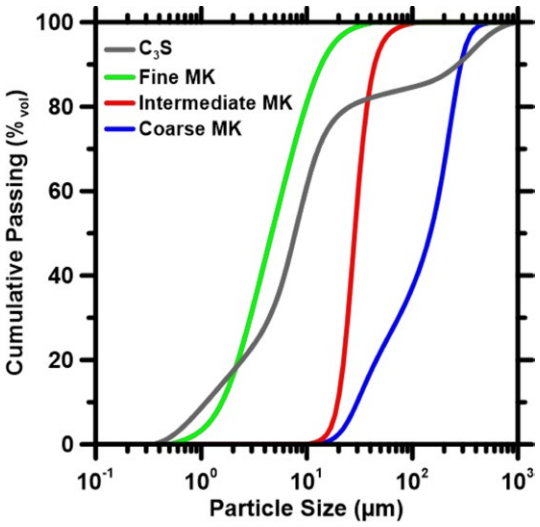

FIGURE 1 The PSDs of C_3S and MK used in this study. The largest relative uncertainty in median diameter (d_{50}, μm) of the powders is on the order of ± 6%

impulse for 30 seconds to prevent agglomeration. Results obtained from PSD determinations are shown in Figure 1. The median particle size (d_{50}) for fine, intermediate, and coarse MK are 4.6200, 28.530, and 148.00 μm, respectively. By factoring the bulk density of MK (ie, 2550 kg/m^3), the SSAs of fine, intermediate, and coarse MK were estimated to be 672, 80, and 29 m^2/kg, respectively. For the C_3S powder, the d_{50} and SSA were 7.78 μm and 562 m^2/kg, respectively; the density of C_3S was assumed to be 3150 kg/m^3. It is clarified that estimations of SSA from PSD are premised on the assumptions that all particulates are spherical, and that the effects of topographical roughness and internal porosity[57–61] on the overall SSA are negligible.[62,63] Because of these assumptions, the SSAs reported above are expected to be smaller than those derived from the Brunauer-Emmett-Teller method.[62,63]

[C_3S + MK] pastes were prepared by mixing the powders with deionized water at a fixed liquid-to-solid mass ratio (*l/s*) of 0.45. The mixing protocols (ie, rate and time of mixing) were kept consistent for all pastes. In binary (ie, [C_3S + MK]) pastes, C_3S was partially replaced by MK (for each of the three PSDs) at two different mass replacement levels: low (ie, 8%$_{mass}$) and high (ie, 30%$_{mass}$). In such pastes, the mass-based water-to-C_3S ratios (*w/c*) are 0.450, 0.489, and 0.643 for 0%$_{mass}$ (control system), 8%$_{mass}$, and 30%$_{mass}$ replacements by MK, respectively. It is clarified that in preparation of the pastes, the utilization of dispersants (eg, high-range water reducing chemical admixtures such as polycarboxylate ether polymer) was avoided. This is because the provision of dispersant could result in complex alterations in C_3S dissolution behavior and nucleation and growth of the hydrates[16] that would be difficult to sequester (and subsequently analyze) from the effect of particulate dispersion (or suppressed agglomeration of particulates) brought about by the dispersant. Hydration kinetics of C_3S in the pastes were monitored for 72 hours after mixing using a TAM IV (TA Instruments) isothermal conduction microcalorimeter, programed to maintain a constant temperature of 20°C ± 0.1°C. Heat evolution profiles collected from the microcalorimetry experiments were processed—using a method employed in several prior studies[9,48,50,64]—to determine the degree of reaction (α, fraction of C_3S that has undergone hydration) and the rate of reaction ($d\alpha/dt$, units of h^{-1}) of C_3S; the enthalpy of hydration[48,64–66] of C_3S used for such analyses was 484 J g_{C3S}^{-1}. To monitor the dissolution dynamics of MK in C_3S paste environments, separate microcalorimetry experiments were conducted on pastes prepared by mixing MK (for all three PSDs) with saturated lime solution at *l/s* of 0.45. Heat evolution profiles collected from such experiments were processed in two steps, as described in prior studies,[9,16] to firstly determine the enthalpy of dissolution of MK, and to subsequently estimate the degree of reaction (α) for MK by plugging in the enthalpy of dissolution.

For identification and quantification of hydrates (ie, C–S–H and CH) and calcite (if any) in pastes, a SDT-Q600 thermogravimetric analyzer (TGA) was used. For arresting hydration of C_3S in such pastes, hydrated samples (after undergoing hydration for 72 hours) were firstly crushed, and then submerged in isopropanol for 24 hours. In some cases, the samples were kept in isopropanol for longer periods; in such cases, "fresh" isopropanol was used to replenish the old one periodically (ie, after every 24 hours). Prior to conducting the TGA experiments, the bulk isopropanol was drained, and the samples were oven-dried at 85°C for an hour. During the TGA experiments, the samples were placed in an Al_2O_3 crucible and heated from room temperature to 1000°C, at a temperature ramp rate of 10°C/min. N_2 gas, passing at a constant flow rate of 100 mL/min, was used to maintain an inert atmosphere within the TGA apparatus. The mass loss (TG) and the differential mass loss (DTG) patterns, derived from the experiments, were used to quantify the amount of CH and calcite (if any) in the samples. For such phase quantifications, methods delineated in prior studies[67,68] were adopted.

3 | PHASE BOUNDARY NUCLEATION AND GROWTH MODEL

A modified phase boundary nucleation and growth (pBNG) model was used to simulate hydration kinetics of C_3S and [C_3S + MK] pastes. The pBNG model has been used in prior studies.[9,16,50,64,66] Therefore, to avoid replication of information, in this section, the underlying assumptions and principles of the pBNG model, and their mathematical formulations, are presented in brief; for further details, readers are requested to refer to references.[9,50]

The pBNG model simulates C_3S hydration as a process driven by heterogeneous nucleation and growth of a single hydration product (ie, C–S–H) of a fixed density.[69,70] Product nucleation is assumed to occur under *site saturation* conditions—wherein all product nuclei form at a given nucleation event, and the product nucleation rate is zero at all times after such event. Once nucleated, the product subsequently grows heterogeneously on solid substrate boundaries (in this case, on C_3S and MK particulates' surfaces). Growth of the product is permitted in all directions except into the substrate.[69,70]

The degree of hydration of C_3S as a function of time, $\alpha(t)$, is calculated from Equation 1. Here, B (unitless) envelops the paste's characteristics (ie, density of components, chemical shrinkage, and *w/c*), and the function $X(t)$ describes the temporal evolution of volume fraction of reactant transformed into hydrate (Equation 2).[16,66,69–71]

$$\alpha(t) = B.X(t) \tag{1a}$$

$$B = \left[\left(\frac{\frac{\rho_{C_3S}}{\rho_{products}}}{\frac{\frac{w}{c}\bullet\rho_{C_3S}}{\rho_{water}}+1}\right)\left(\frac{c+\frac{1}{\rho_{C_3S}}-\frac{1}{\rho_{water}}}{\frac{1}{\rho_{product}}-\frac{1}{\rho_{water}}}\right)\right]^{-1} \quad (1b)$$

$$X(t) = 1 - \exp\left[-2k_G\cdot(t-\tau)\cdot\left(1-\frac{F_D\left[k_s\cdot(t-\tau)\right]}{k_s\cdot(t-\tau)}\right)\right] \quad (2)$$

In Equation 2, F_D is the f-Dawson function. The variables k_s (h^{-1}) and k_g (h^{-1}) are functions of nucleation density ($I_{density}$, μm^{-2}) and outward growth rate [G_{out} (t), μm/h] of the product (see References [9,50] for more details). It should be noted that in the pBNG model, the growth of the product is assumed to occur in an anisotropic fashion, while varying with respect to time. In the lateral direction (ie, parallel to the substrate's surface), the growth rate is isotropic; however, in the longitudinal direction (ie, perpendicular to the substrate's surface), the outward growth rate (G_{out}) is double the rate in the lateral direction. Such anisotropy in product's growth has been implemented to mimic the actual geometry of C–S–H's early-age growth, as observed in experiments.[72,73] The temporal variation in growth rate is based on an implementation originally formulated by Bullard et al,[71] and subsequently adopted in several studies,[9,16,50,64,66] to capture changes in C–S–H's growth rate in relation to its supersaturation in the solution.

By coupling the product nucleation density with the substrate's (ie, of C_3S and MK particulates) overall specific surface area (SSA_{solid}, $m^2\ kg_{C3S}^{-1}$, as shown in Equations 3 and 4), the number of supercritical product nuclei per unit mass of C_3S in the paste (N_{Nuc}, kg_{C3S}^{-1}) can be estimated.[9,16,74] Here, a_{MK} (unitless) acts a free simulation variable[9] that represents the reactive area fraction of MK, that is, the area fraction not affected by particulate agglomeration and/or other ion-specific effects (eg, inhibition due to aluminate-ion adsorption). The other parameter, z ($\%_{mass}$), represents the replacement level of C_3S by MK in the paste.

$$N_{Nuc} = SSA_{solid} I_{density} \quad (3)$$

$$SSA_{solid} = SSA_{C_3S} + a_{MK}\, SSA_{MK} \frac{z}{(100-z)} \quad (4)$$

Within the pBNG framework, as described above and in references,[9,50] the variables that need to be ascertained for reproduction of the measured reaction rates are: $G_{out}(t)$, $I_{density}$, and a_{MK}. A Nelder-Mead-based simplex algorithm[75] is used to determine optimum values of these variables in two steps. In the first step, G_{out} is fixed at 0.075 μm/h (a value derived from scanning transmission electron microscopy[72,73,76]) whereas $I_{density}$ and a_{MK} are allowed to vary. The first step yields optimum values of $I_{density}$ and a_{MK}, which are subsequently used in the second step to estimate the optimal functional form of G_{out} (t). It is clarified that during the aforementioned optimizations, convergence is assumed to have reached when: (a) the deviation between measured and simulated reaction rates are within 1%; and (b) the simulation output does not change by more than $\pm 10^{-6}$ units in three successive simulation steps.

4 | RESULTS AND DISCUSSION

4.1 | Effect of PSD of metakaolin on hydration kinetics of C_3S

Figure 2 shows heat evolution profiles of [C_3S + MK] pastes, prepared by replacing 8$\%_{mass}$ of C_3S with MK. As

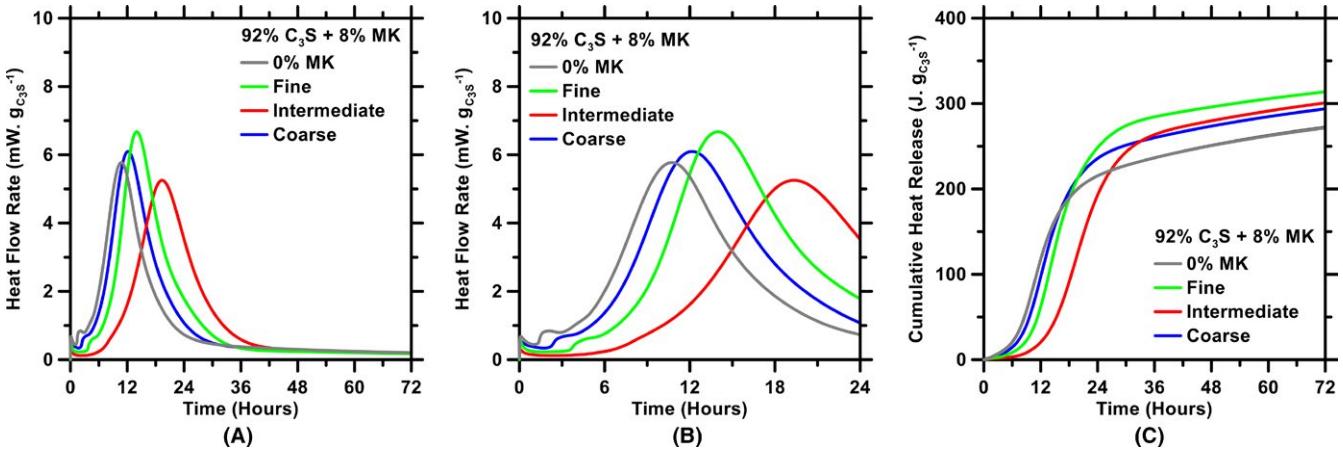

FIGURE 2 Measured calorimetry profiles of [C_3S + MK] pastes, wherein 8$\%_{mass}$ of C_3S is replaced by MK. Three different PSDs of MK have been used. (A) Heat flow rates up to 72 h of hydration; (B) heat flow rates up to 24 h of hydration; and (C) cumulative heat release up to 72 h of hydration. The *l/s* of all pastes is 0.45. For a given system, the uncertainty in the measured heat flow rate at the main hydration peak is ±2%

can be seen in Figure 2A, at low replacement level, both fine and coarse MK produce greater peak heat flow rates (ie, heat flow rates at the main hydration peaks) compared to the control (ie, pure C_3S) paste. This is indicative of the "filler effect," wherein provision of additional solid surface area by the additive's (ie, MK's) particulates results in creation of supplementary sites for heterogeneous nucleation and subsequent growth of C–S–H.[9,10,15,49] Unlike the fine and coarse MK, the intermediate MK suppresses nucleation and growth of C–S–H, as evidenced by lower peak flow rate compared to the control paste. While the peak heat flow rates (and, therefore, alterations in C_3S hydration kinetics) do not exhibit monotonic relationship with fineness of MK particulates, all three [C_3S + MK] pastes reliably show prolongation of the induction period as compared to the control paste (Figure 2B). The intermediate MK prompts the largest extension in the induction period, followed by the fine and coarse MK, respectively. Such prolongation of the induction period results in lower early-age (eg, at 12 hours) cumulative heat release in all [C_3S + MK] pastes compared to that of the control paste (Figure 2C). As cumulative heat release is a direct indicator of degree of reaction of C_3S, it can be said that provision of MK in the paste results in lower degree of C_3S hydration at early ages. Notwithstanding, at the age of 72 hours, the cumulative heat release of each of three [C_3S + MK] pastes surpasses that of the control paste. This is because in [C_3S + MK] pastes, the post-peak deceleration is slower (see Figure 2B), and, therefore, C_3S hydration kinetics beyond the peak are faster (ie, heat flow rates are higher) compared to that of the control paste. In summary, at low replacement level of MK and at later ages (ie, age ≈72 hours), the degree of C_3S hydration in binary pastes is superior compared to the control paste.

At high replacement level (ie, 30%$_{mass}$) of C_3S with MK, hydration of the host material is suppressed (see Figure 3A), regardless of the PSD of MK, throughout the 72 hours after mixing. This is better shown in Figure 3B, which focuses on the first 24 hours of hydration. As can be seen, all three PSDs of MK cause substantial prolongation of induction period, delayed occurrence of the main hydration peak, slower acceleration to the peak, and lower peak heat flow rate as compared to the control paste. Akin to results of [C_3S + 8%$_{mass}$ MK] pastes shown in Figure 2, the intermediate MK has the most prominent effect on C_3S hydration among all [C_3S + 30%$_{mass}$ MK] pastes, as evidenced by the protracted induction period, lowest slope of acceleration to the peak, and the greatest delay in occurrence of the main hydration peak (Figure 3B). Also, due to the lower slope of post-peak deceleration (ie, slower departure from the main hydration peak), the degrees of C_3S hydration in all [C_3S + MK] pastes surpass that of the control paste at 72 hours (Figure 3C). Therefore, based on the results shown in Figure 3, it can be said that at high replacement level of MK, regardless of the PSD (or SSA) of the additive's particulates, hydration of C_3S is suppressed at early ages. Such suppression of C_3S hydration, however, progressively diminishes with age, and ultimately reverses producing greater degrees of C_3S hydration in binary pastes compared to the control paste.

The inferences of degree of reaction of C_3S in [C_3S + MK] pastes made from the cumulative heat release profiles (Figures 2and 3) are qualitative in nature. For quantitative estimates, portlandite (ie, CH) contents in the pastes were measured, and plotted (Figure 4A,B). The results were found to be in very good agreement with inferences made from the heat evolution profiles. As can be seen, at both low and high replacement levels, the intermediate

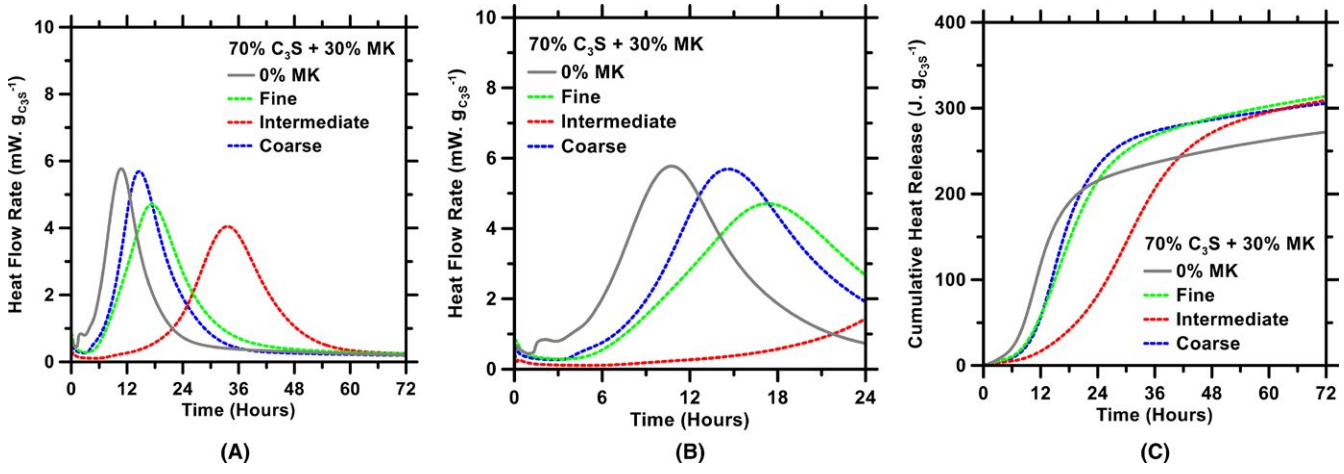

FIGURE 3 Measured calorimetry profiles of [C_3S + MK] pastes, wherein 30%$_{mass}$ of C_3S is replaced by MK. Three different PSDs of MK have been used. (A) Heat flow rates up to 72 h of hydration; (B) heat flow rates up to 24 h of hydration; and (C) cumulative heat release up to 72 h of hydration. The *l/s* of all pastes is 0.45. For a given system, the uncertainty in the measured heat flow rate at the main hydration peak is ±2%

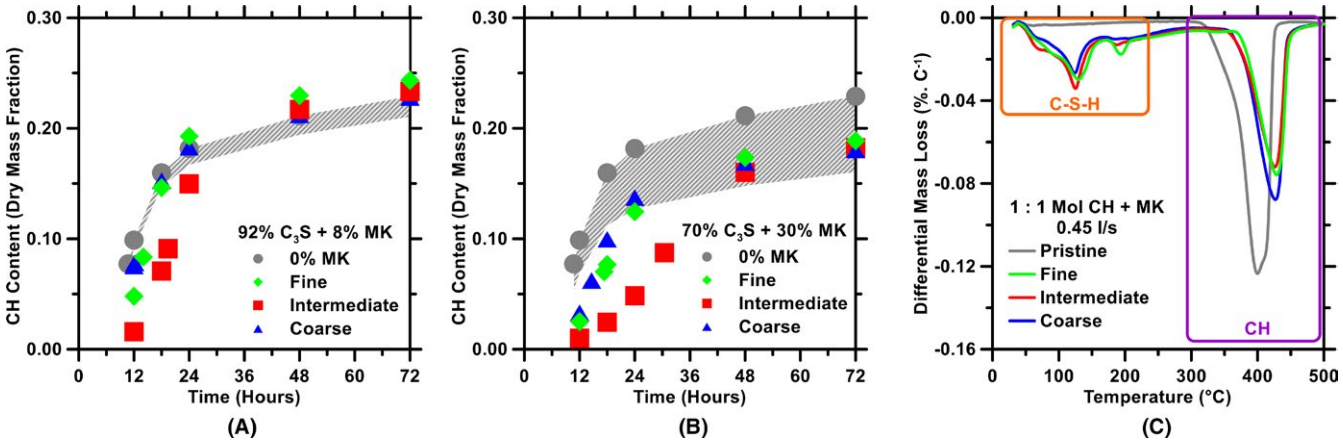

FIGURE 4 The temporal evolution of CH content (expressed as dry mass fraction) in [C_3S + MK] pastes, prepared at: (A) 8% replacement; and (B) 30% replacement level of C_3S with MK. The upper bound of the gray area represents the CH content formed in the control paste, and the lower bound represents the dilution line (ie, proportional reduction in CH content in relation to the reduction in C_3S content). (C) DTG traces showing differential mass loss, as function of temperature, in a [MK + CH (1:1 molar ratio)] paste (*l/s* = 0.45) at 72 h after mixing. The highest uncertainty in phase quantifications by DTG is ±2.5%

MK suppresses early-age (ie, up to ≈24 hours) hydration of C_3S the most. This is evidenced by CH contents that are consistently lowest among all pastes, and even below the dilution line (which represents the proportional decrease in CH content with respect to decreasing C_3S content in binary paste). At the age of 72 hours, however, the CH contents in binary pastes—regardless of the PSD of MK—are above the dilution line. This corroborates the argument made earlier in this section that the MK-induced suppression of C_3S hydration, observed at early ages, is reversed at later ages. More importantly, as CH contents of binary pastes invariably stay above the dilution line (at 72 hours, see Figure 4A,B), it can be said that the pozzolanic reaction between MK (regardless of its PSD) and CH within the first 72 hours of hydration is not significant. This is in very good agreement with findings of prior studies,[42,77–79] and strongly suggests that within the first 72 hours after mixing, the impact of pozzolanic activity of MK on hydration behavior of C_3S in [C_3S + MK] pastes is insignificant. It is worth clarifying that the poor pozzolanic activity of MK in [C_3S + MK] pastes is not exclusively due to the slower dissolution dynamics of MK (this is further described in Section 4.2). Rather, the limiting factor is expected to be the low content of CH in such binary pastes. To corroborate this, additional TGA experiments were conducted to examine the reduction in CH content and the resultant formation of pozzolanic C–S–H in [MK + CH, at 1:1 molar ratio] pastes, prepared by mixing MK and CH with water at *l/s* of 0.45. As can be seen in Figure 4C, when adequate amount of CH is present, the pozzolanic reaction of MK with CH is substantial (ie, up to 20%$_{mass}$ reduction in CH content, and formation of pozzolanic C–S–H in equivalent amount). This suggests that in a mature [C_3S + MK] paste (ie, after age» 72 hours), when substantial amount of CH is present, the pozzolanic activity of MK is expected to upsurge.

Heat flow rate profiles, shown in Figures 2 and 3, qualitatively contrast C_3S hydration kinetics in [C_3S + MK] pastes in relation to PSD and replacement level of MK. To gain proper, quantitative understanding, additional data (ie, calorimetric parameters[9,10,16,64]: inverse of time to the peak (h^{-1}), maximum heat flow rate (mW g_{C3S}^{-1}), and slope of the acceleration regime (mW g_{C3S}^{-1} h^{-1})) were extracted from the heat evolution profiles, consolidated, and plotted (Figure 5).

As can be seen (Figure 5A), the main hydration peak is delayed in all binary pastes; the delay magnifies as the MK content in the paste increases. In a prior study,[9] it was reported that such prolongation of the induction period is directly related to the release of aluminate (ie, $[Al(OH)_4^-]$) ions from the dissolution of MK. More specifically, the adsorption of aluminate ions onto C_3S particulates' surfaces blocks dissolution sites (eg, kinks on etch pits of C_3S surfaces[43]). This, in turn, slows C_3S dissolution dynamics and prolongs the induction period. Expectedly, these effects of aluminate-ion adsorption (which leads to inhibited dissolution of C_3S) become progressively more pronounced as the content of MK in the paste increases (Figure 5A). This hypothesis—that the aluminate ions passivate the surface of C_3S particulates—is supported by results obtained from prior studies focused on C_3S hydration in the presence of slightly or highly soluble aluminum-based[43–47] or aluminosilicate compounds.[81–83] Using molecular dynamics simulations, Pustovgar et al[43] showed that the absorption of aluminate anions onto C_3S particulates' surfaces is energetically favorable due to formation of aluminosilicate complexes, comprising of ionic and hydrogen bonds between the aluminate ions and Ca^{2+} and OH^- ions (that remain in the vicinity to C_3S particulate surfaces forming an electric double-layer). As C_3S continues to dissolve

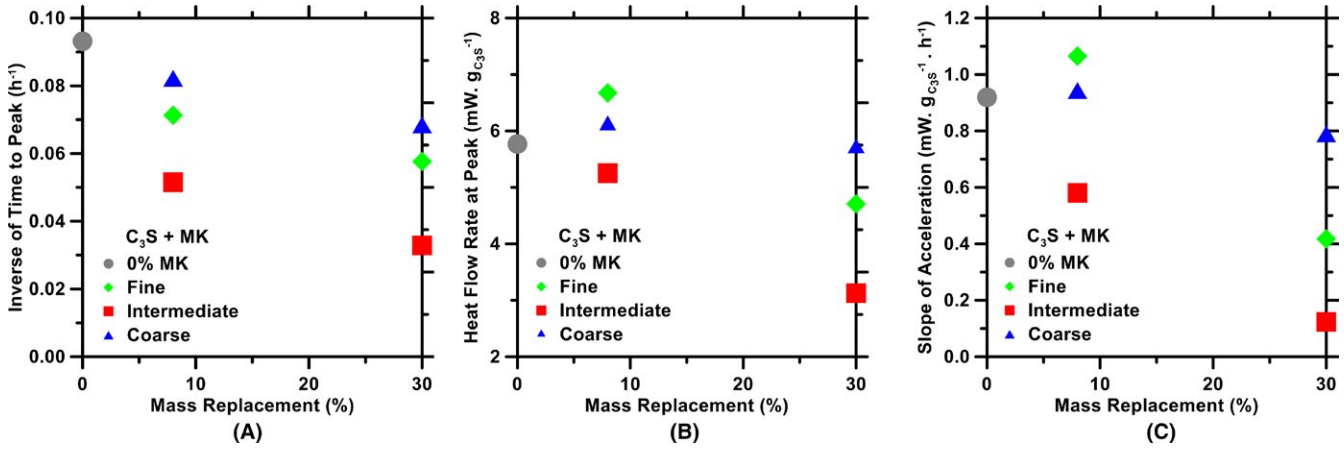

FIGURE 5 Calorimetric parameters extracted from heat evolution profiles of pastes: (A) inverse of time to the main hydration peak; (B) heat flow rate at the main hydration peak; and (C) slope of the acceleration period. The uncertainty in each calorimetric parameter is the same as the uncertainty in calorimetry profiles, that is, ±2%

(though at a slower rate), the pH of the contacting solution continues to increase. At a critical pH, when the concentrations of Ca^{2+} and OH^- ions in the solution are elevated to CH saturation level (ie, pH ≈ 12.68[43]), the aforementioned aluminosilicate complexes on C_3S surfaces become thermodynamically unstable; as a result, the aluminate ions desorb from C_3S surfaces.[43] This event is marked by termination of the induction period and onset of the acceleration regime. In Figure 5A, it is interesting that although the intermediate MK does not have the largest SSA, its ability to passivate C_3S surface (and, therefore, it's potential to prolong the induction period and delay the main hydration peak) is superior compared to the fine (with largest SSA) and coarse (with lowest SSA) MK. Since the ability to passivate C_3S surface is directly linked with the release of aluminate ions, it is hypothesized that the intermediate MK has the fastest dissolution rate in C_3S paste environments. This hypothesis will be corroborated later in Section 4.2.

Going back to Figure 5, it can be seen that at low replacement level, fine and coarse MK produce higher peak heat flow rates (Figure 5B) and slopes of acceleration regimes (Figure 5C) compared to the control paste. In contrast, at high replacement level, both calorimetric parameters are lower than those of the control paste. These results, therefore, suggest that at low replacement level, both the fine and coarse MK act as fillers, and enhance nucleation and growth of C–S–H through provision of additional nucleation sites on their surfaces. At high replacement level, however, the ability of MK to serve as a filler is not just diminished but reversed. As reported in a prior study,[9] this reversal in MK's filler effect is attributed to the higher concentration of aluminate ions (resulting from dissolution of MK) in the solution of such pastes. The large abundance of aluminate ions causes passivation of MK particulates' surfaces in addition to those of C_3S particulates. Such passivation blocks C–S–H nucleation sites on MK surfaces, thus diminishing and ultimately reversing (akin to "poisoning" of) its filler effect. Figure 5B,C clearly show that, among the three PSDs of MK, the intermediate MK suppresses C–S–H nucleation and growth the most. This suggests that the intermediate MK is most proficient (compared to the other PSDs of MK) at releasing aluminate ions in the solution, which essentially lies at the origin of suppression of C_3S dissolution (Figure 5A) and C–S–H nucleation and growth (Figure 5B,C).

4.2 | Effect of PSD on dissolution dynamics of MK

The hypotheses derived from the results presented in Section 4.1 are premised on one central concept that of all PSDs of MK (ie, fine, intermediate, and coarse), the intermediate one has the fastest dissolution dynamics, and, consequently, prompts the fastest release of aluminate ions into the contacting solution. It has been argued that greater abundance of aluminate ions in pore solution of [C_3S + intermediate MK] paste is the principal reason for C_3S hydration suppression. To test the veracity of the concept, additional calorimetry experiments were conducted to monitor the dissolution dynamics of MK in saturated lime solution. The solvent was chosen to be DI-water saturated with calcium hydroxide [ie, $Ca(OH)_2$], because several past studies[48,65,66,71,84,85] have shown that in C_3S pastes, following a few hours after mixing, the pore-solution [consisting of Ca^{2+}, OH^- ions at millimolar (mmol/L) levels, and $H_2SiO_4^{2-}$/$H_3SiO_4^-$ ions at micromolar (μmol/L) level] composition remains in vicinity of $Ca(OH)_2$ saturation level for protracted periods.

As can be seen in Figure 6, the intermediate MK, indeed, dissolves faster, and to greater extents, than the fine and coarse MK throughout the 168 hours after mixing. Based

on the SSAs of the PSDs of MK (reported in Section 2.0), it would be expected that dissolution dynamics would be fastest for the fine, followed by the intermediate and then by the coarse MK. The results shown in Figure 6 are, therefore, counterintuitive as the dissolution kinetics do not appear to follow a monotonic relationship with SSA of MK particulates. Although the exact reasons for this anomaly are not known, it is expected that slower dissolution kinetics of the fine MK is due to the following reasons: (a) agglomeration of its fine particulates, which, in turn, results in significant reduction of overall surface area, thus causing deceleration of dissolution kinetics; and (b) passivation of MK particulates' surfaces, caused by aluminate ions released from the initial (and rapid) burst of dissolution of the fine particulates. The intermediate MK, which comprises of particulates between 20 and 32 μm, has lower SSA compared to the fine MK, but is not expected to be susceptible to agglomeration. As such, it is possible that the "reactive surface area" (ie, surface area that is unaffected by particle agglomeration or aluminate-ion adsorption, and, therefore, able to partake in dissolution) of intermediate MK is larger than that of fine MK (and coarse MK), resulting in the fastest dissolution kinetics. Validation of this hypothesis is provided in Section 4.3 with the aid of simulations conducted using the pBNG model.

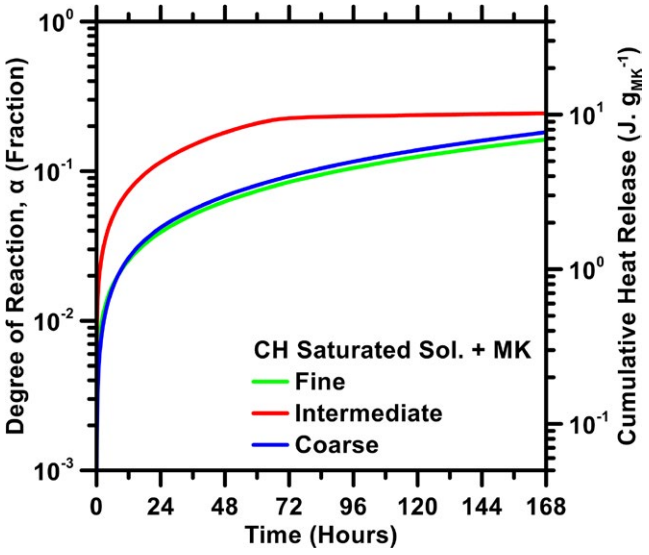

FIGURE 6 Isothermal microcalorimetry-based determinations of time-dependent degree of reaction (primary y-axis) and cumulative heat release (secondary y-axis) of MK dissolving in saturated lime solution. For such low-heat evolving systems, the uncertainty in the measured heat flow rate at any given point in time is within ±5%

4.3 | Numerical Simulations of Hydration Kinetics of [C_3S + MK] Pastes

To gain further insights into the role of PSD of MK on C_3S hydration kinetics, the pBNG model (described in Section 3.0) was employed. Experimentally derived reaction rates (ie, $d\alpha/dt$, calculated from calorimetry profiles) of pastes were used as inputs. The simplex algorithm, embedded within the pBNG model, was invoked to reproduce the input profiles by optimizing the following simulation variables: product nucleation density ($I_{density}$), reactive area fraction of MK participating in product nucleation (a_{MK}), and the time-dependent outward growth rate of product [G_{out} (t)]. Through such optimizations, the pBNG model was able to reproduce the experimental results (figure not shown). Optimum values of the aforementioned simulation parameters, for the different pastes, were subsequently consolidated, and plotted (Figure 7).

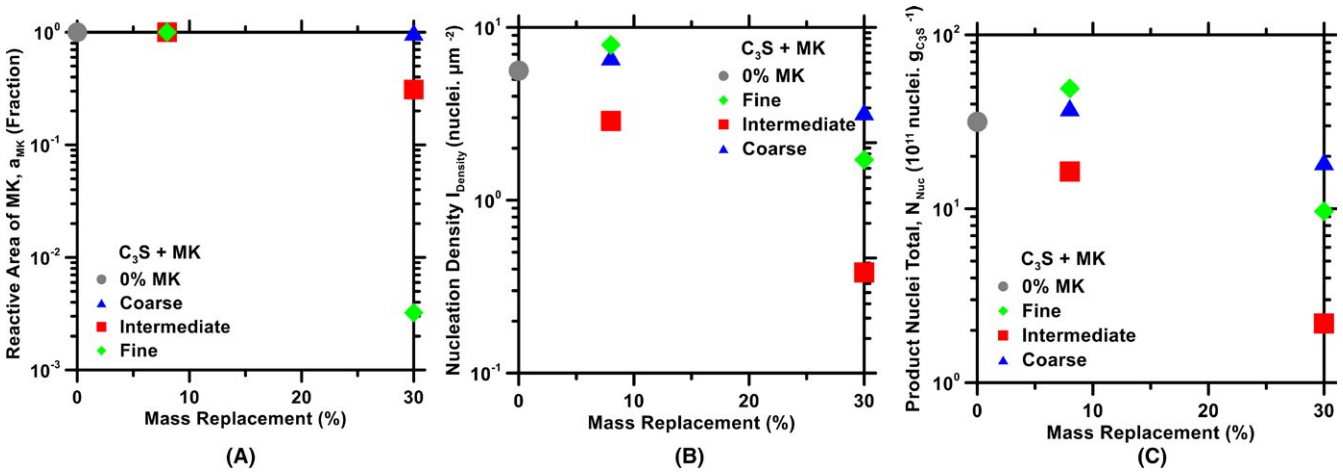

FIGURE 7 Parameters derived from pBNG simulations of [C_3S + MK] pastes: (A) reactive area fraction of MK (a_{MK}); (B) product nucleation density ($I_{density}$); and (C) total number of product nuclei per gram of C_3S (N_{Nuc}). All parameters are plotted against the MK replacement level ($\%_{mass}$) in the pastes. Simulations are deterministic, and, therefore, there is no uncertainty associated with them

Figure 7A,B show variations in a_{MK} and $I_{density}$, respectively, in relation to the MK replacement level. The plots show that at low replacement level (ie, 8%$_{mass}$), majority of surface area of MK particulates—regardless of the PSD of MK—is available for C–S–H nucleation. In accordance with this, both the fine and coarse MK serve as fillers and enhance heterogeneous nucleation of C–S–H on their particulates' surfaces (see Figure 7B). Due to its higher SSA, expectedly, the fine MK enhances $I_{density}$ more than the coarse MK. The intermediate MK, however, causes a decline in $I_{density}$—a clear reversal of the filler effect. This reversal is attributed to its faster dissolution kinetics (see Figure 6), which causes rapid release of aluminate ions into the contacting solution. The aluminate ions, in due time, adsorb onto C_3S and MK particulates' surfaces, thus blocking potential C–S–H nucleation sites.

At high replacement level (ie, 30%$_{mass}$), a large fraction of surface area of fine MK (with the largest SSA) is unable to partake in the nucleation and growth process (Figure 7A); furthermore, $I_{density}$ is significantly lower compared to the control paste (Figure 7B). These results are in good agreement with the discussion in Section 4.2, wherein it was hypothesized that in fine MK, effects of particle agglomeration and (aluminate ion induced) passivation of particulates' surfaces result in significant diminishment of reactive surface area and blockage of potential sites for C–S–H nucleation. Notably in the [C_3S + intermediate MK] paste, at 30%$_{mass}$ replacement level of MK, ≈70% of the surface area is rendered unreactive (Figure 7A) and $I_{density}$ is reduced by ≈1 order of magnitude with respect to the control paste (Figure 7B). Such large reductions in a_{MK} and $I_{density}$ are attributed exclusively to the passivation caused by rapid release (Figure 6) and subsequent adsorption of aluminate ions onto the MK particulates' surfaces; particulate agglomeration is expected to be negligible in the intermediate MK. The reduction in $I_{density}$ of [C_3S + coarse MK] paste—albeit small—is also attributed solely to the surface passivation induced by aluminate ions.

The two simulation parameters, a_{MK} and $I_{density}$, were combined [as described in Section 3.0 (Equation 3)] to estimate the total number of supercritical product nuclei formed at the nucleation event (N_{Nuc}: Figure 7C). As can be seen, the trends in N_{Nuc} with respect to MK replacement level are remarkably similar to those exhibited by calorimetric parameters (shown in Figure 4) extracted directly from experiments. It is posited that such similarity between experiments and simulations validates the pBNG model and its implementation. Figure 7C shows that at low replacement level, the fine and coarse MK are able to exert filler effect and enhance the number of C–S–H nuclei in the paste. At high replacement level, owing to the reduction in reactive surface area of MK particulates (Figure 7A) and concurrent reduction in $I_{density}$ (Figure 7B), the values of N_{Nuc} of all [C_3S + MK] pastes remain consistently below the control paste. The intermediate MK, in particular, significantly reduces N_{Nuc}, almost by an order of magnitude with respect to the control paste. This corroborates the hypothesis that faster dissolution kinetics of intermediate MK (as shown previously in Figure 6) results in faster release of aluminate ions, which then passivate the substrates' surfaces thus blocking potential C–S–H nucleation sites.

The other simulation parameter optimized from pBNG simulations is the outward product growth rate [$G_{out}(t)$] (Figure 8). This functional form of G_{out} has been reported[9,50,64,71] to emulate evolution of C–S–H supersaturation in the solution. It is noted that, at early ages (ie, up to ≈12 hours), G_{out} of [C_3S + 8%$_{mass}$ MK] and [C_3S + 30%$_{mass}$ MK] pastes are lower than those of the control paste. This suggests that MK not only suppresses nucleation of C–S–H, but also its post-nucleation growth. Although the exact mechanisms for this are not understood, it is speculated, as has also been suggested in a prior study,[9] that the residual aluminate ions present in the solution (ie, ions that are not adsorbed onto substrates' surfaces during the first few hours of hydration) adsorb onto C–S–H and, subsequently cut off its access to the contiguous solution, thus subduing its growth. When the paste is mature (ie, age ≈72 hours), that is, when the supersaturation of C–S–H is relegated to low values,[50,71,85] such effects of aluminate ions on product growth rate become less discernible. As such, G_{out} converges to similar (and low) values regardless of the PSD or replacement level of MK.

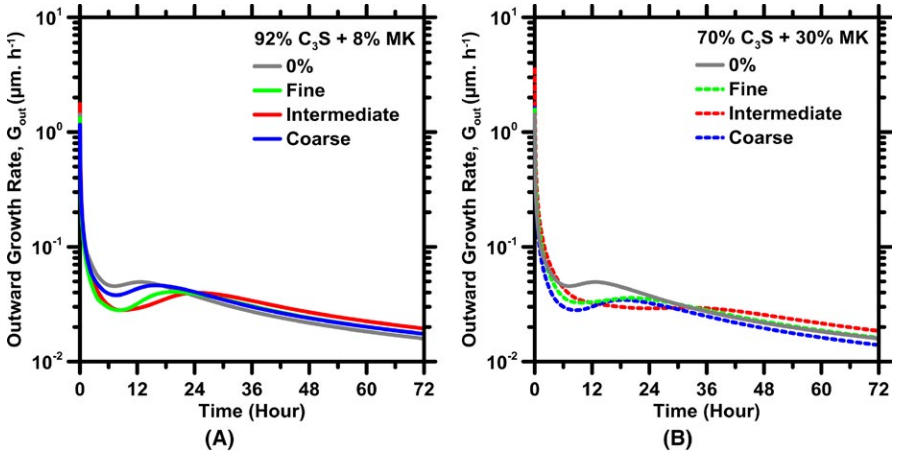

FIGURE 8 Simulation output, outward growth rate of the product, in (A) [C_3S + 8%$_{mass}$ MK]; and (B) [C_3S + 30%$_{mass}$ MK] pastes as function of time. Simulations are deterministic, and, therefore, there is no uncertainty associated with them

Overall, the results reported and discussed in Sections 4.1-4.3 show that within the first 72 hours of hydration of [C_3S + MK] pastes, the pozzolanic activity of MK is insignificant (see Figure 4), and, therefore, unable to affect C_3S hydration behavior in a consequential way. MK, however, has the potential to serve as a filler, but magnitude of its filler effect is strongly dependent on its PSD and content in the paste. Importantly, this study shows that a mere increase in SSA of MK particulates (eg, achieved using grinding methods) does not lead to proportional or monotonic enhancement of the filler effect as it does for other inert fillers (eg, limestone and quartz[8,10,49]).

5 | CONCLUSIONS

This study attempts to elucidate the effect of particle size distribution (PSD) of metakaolin (MK) on hydration kinetics of tricalcium silicate (C_3S) during the first 72 hours after mixing. Three unique PSDs—fine, with particulate sizes <20 μm; intermediate, with particulate sizes between 20 and 32 μm; and coarse, with particulate sizes >32 μm—of MK were used. The additive was used to partially replace C_3S in pastes (prepared as constant liquid-to-solid mass ratio of 0.45); two different replacements [ie, low ($8\%_{mass}$) and high ($30\%_{mass}$)] were used. Isothermal microcalorimetry, in conjunction with TGA, was used to monitor kinetics of C_3S hydration in the pastes. A phase boundary nucleation and growth model was applied to reproduce the experimentally derived hydration kinetics profiles, and assess variations in key nucleation and growth parameters in relation to the PSD and content of MK in the pastes.

The results show that—unlike other fillers such as limestone and quartz—the correlation between SSA of MK's particulates and the consequent alteration in hydration behavior of C_3S is nonlinear and nonmonotonic. MK is able to exert filler effect, albeit the magnitude of the filler effect depends strongly on the PSD and content of MK. Very fine (high SSA) or coarse (low SSA) particulates of MK are able to exert filler effect at low replacement level. The filler effect manifests as enhanced nucleation density of C–S–H, resulting in faster kinetics of C_3S hydration in neighborhood of the main hydration peak. At high replacement level, however, the filler effect of MK is reversed. This is due to effects of particulate agglomeration (especially, in the case of fine MK) and aluminate [$Al(OH)_4^-$] ion induced surface passivation (in both coarse and fine MK). The surface passivation effect is caused by adsorption of aluminate ions (released from the dissolution of MK into the solution) onto C_3S and MK particulates, which inhibit C–S–H nucleation sites on the substrates' surfaces and suppress the post-nucleation growth of C–S–H.

In the case of intermediate MK, the SSA of which intermediates between those of coarse and fine MK, the filler effect is observed neither at low nor at high replacement levels. In fact, the filler effect is reversed even at low replacement level, and the nucleation density of C–S–H is diminished progressively (with respect to the control paste) as the content of MK in the paste increases. This is due to faster dissolution kinetics of intermediate MK, which results in faster release of aluminate ions in the solution, and, therefore, more pronounced inhibition of C_3S dissolution and C–S–H nucleation sites.

Overall, outcomes of this work provide new insights into the role of particle size of MK on hydration mechanisms of C_3S. For the first time, it is shown that grinding-based improvements in specific surface area (or fineness) of MK particulates does not necessarily result in enhanced early-age hydration of C_3S. The results, which are rather counterintuitive, strongly suggest that low replacement level of MK, wherein particulates of MK are predominantly coarse (ie, low SSA), are optimal for enhancement of hydration of C_3S (ie, up to 72 hours). This is because coarse MK particulates are least susceptible to effects of particulate agglomeration and aluminate ions-induced surface passivation.

ACKNOWLEDGMENTS

This study was conducted in the Materials Research Center (MRC) of Missouri University of Science and Technology (Missouri S&T). The authors acknowledge the financial support provided by the National Science Foundation (NSF, CMMI: 1661609 and CMMI: 1761697). The authors declare no conflict of interest.

ORCID

Jonathan Lapeyre https://orcid.org/0000-0003-2562-7005
Hongyan Ma https://orcid.org/0000-0003-3674-3845
Aditya Kumar https://orcid.org/0000-0001-7550-8034

REFERENCES

1. Antoni M, Rossen J, Martirena F, Scrivener K. Cement substitution by a combination of metakaolin and limestone. Cem Concr Res. 2012;42(12):1579–89.
2. Juenger M, Winnefeld F, Provis JL, Ideker JH. Advances in alternative cementitious binders. Cem Concr Res. 2011;41(12):1232–43.
3. Meyer C. The greening of the concrete industry. Cem Concr Compos. 2009;31(8):601–5.
4. Worrell E, Price L, Martin N, Hendriks C, Meida LO. Carbon dioxide emissions from the global cement industry. Annu Rev Energy Environ. 2001;26(1):303–29.
5. Gartner E. Industrially interesting approaches to "low-CO_2" cements. Cem Concr Res. 2004;34(9):1489–98.
6. Biernacki JJ, Bullard JW, Sant G, Brown K, Glasser FP, Jones S, et al. Cements in the 21st century: challenges, perspectives, and opportunities. J Am Ceram Soc. 2017;100(7):2746–73.

7. Bich C, Ambroise J, Péra J. Influence of degree of dehydroxylation on the pozzolanic activity of metakaolin. Appl Clay Sci. 2009;44(3–4):194–200.
8. Kumar A, Oey T, Falzone G, Huang J, Bauchy M, Balonis M, et al. The filler effect: the influence of filler content and type on the hydration rate of tricalcium silicate. J Am Ceram Soc. 2017;100(7):3316–28.
9. Lapeyre J, Kumar A. Influence of pozzolanic additives on hydration mechanisms of tricalcium silicate. J Am Ceram Soc. 2018;101(8):3557–74.
10. Oey T, Kumar A, Bullard JW, Neithalath N, Sant G. The filler effect: the influence of filler content and surface area on cementitious reaction rates. J Am Ceram Soc. 2013;96(6):1978–90.
11. Gutteridge WA, Dalziel JA. Filler cement: the effect of the secondary component on the hydration of Portland cement. Part 1: A Fine non-hydraulic binders. Cem Concr Res. 1990;20(6):778–82.
12. Gutteridge WA, Filler D. Cement: the effects of the secondary component on the hydration of portland cement. Part 2. Fine non-hydraulic filler. Cem Concr Res. 1990;20(c):853–61.
13. Lothenbach B, Scrivener K, Hooton RD. Supplementary cementitious materials. Cem Concr Res. 2011;41(12):1244–56.
14. Deschner F, Winnefeld F, Lothenbach B, Seufert S, Schwesig P, Dittrich S, et al. Hydration of Portland cement with high replacement by siliceous fly ash. Cem Concr Res. 2012;42(10):1389–400.
15. Berodier E, Scrivener K. Understanding the filler effect on the nucleation and growth of C–S–H. J Am Ceram Soc. 2014;97(12):3764–73.
16. Meng W, Lunkad P, Kumar A, Khayat K. Influence of silica fume and PCE dispersant on hydration mechanisms of cement. J Phys Chem C. 2016;120(47):26814–23.
17. Idir R, Cyr M, Tagnit-Hamou A. Pozzolanic properties of fine and coarse color-mixed glass cullet. Cem Concr Compos. 2011;33(1):19–29.
18. Wild S, Khatib JM. Portlandite consumption in metakaolin cement pastes and mortars. Cem Concr Res. 1997;27(1):137–46.
19. Shi C, Day RL. Pozzolanic reaction in the presence of chemical activators Part I. Reaction kinetics. Cem Concr Res. 2000;30(1):51–8.
20. Shi C, Day RL. Pozzolanic reaction in the presence of chemical activators Part II. Reaction products and mechanism. Cem Concr Res. 2000;30(4):607–13.
21. Fernandez R, Martirena F, Scrivener KL. The origin of the pozzolanic activity of calcined clay minerals: a comparison between kaolinite, illite and montmorillonite. Cem Concr Res. 2011;41(1):113–22.
22. Tironi A, Trezza MA, Scian AN, Irassar EF. Assessment of pozzolanic activity of different calcined clays. Cem Concr Compos. 2013;37(1):319–27.
23. He C, Oscbaek B, Makovicky E. Pozzolanic reactions of six principle clay minerals: activiation, reactivity assessments and technological effects. Cem Concr Res. 1995;25(8):1691–702.
24. Shi Z, Lothenbach B, Geiker MR, Kaufmann J, Leemann A, Ferreiro S, et al. Experimental studies and thermodynamic modeling of the carbonation of Portland cement, metakaolin and limestone mortars. Cem Concr Res. 2016;88:60–72.
25. Al-Akhras NM. Durability of metakaolin concrete to sulfate attack. Cem Concr Res. 2006;36(9):1727–34.
26. Ramlochan T, Thomas M, Gruber KA. The effect of metakaolin on alkali–silica reaction in concrete. Cem Concr Res. 2000;30(3):339–44.
27. Roy D, Arjunan P, Silsbee M. Effect of silica fume, metakaolin, and low-calcium fly ash on chemical resistance of concrete. Cem Concr Res. 2001;31(12):1809–13.
28. Frías M, Cabrera J. Pore size distribution and degree of hydration of metakaolin–cement pastes. Cem Concr Res. 2000;30(4):561–9.
29. Badogiannis E, Kakali G, Tsivilis S. Metakaolin as supplementary cementitious material : optimization of kaolin to metakaolin conversion. J Therm Anal Calorim. 2005;81(2):457–62.
30. Shvarzman A, Kovler K, Grader G, Shter G. The effect of dehydroxylation/amorphization degree on pozzolanic activity of kaolinite. Cem Concr Res. 2003;33(3):405–16.
31. Sabir B, Wild S, Bai J. Metakaolin and calcined clays as pozzolans for concrete: a review. Cem Concr Compos. 2001;23(6):441–54.
32. Brindley GW, Nakahira M. The Kaolinite-mullite reaction series: II. Metakaolin. J Am Ceram Soc. 1959;42(7):314–8.
33. Brindley GW, Nakahira M. The Kaolinite-mullite reaction series: III, the high-temperature phases. J Am Ceram Soc. 1959;42(7):319–24.
34. White CE, Provis JL, Proffen T, Riley DP, van Deventer J. Combining density functional theory (DFT) and pair distribution function (PDF) analysis to solve the structure of metastable materials: the case of metakaolin. Phys Chem Chem Phys. 2010;12(13):3239.
35. Sperinck S, Raiteri P, Marks N, Wright K. Dehydroxylation of kaolinite to metakaolin—a molecular dynamics study. J Mater Chem. 2011;21(7):2118–25.
36. Taylor-Lange SC, Riding KA, Juenger M. Increasing the reactivity of metakaolin-cement blends using zinc oxide. Cem Concr Compos. 2012;34(7):835–47.
37. Konan KL, Peyratout C, Smith A, Bonnet JP, Rossignol S, Oyetola S. Comparison of surface properties between kaolin and metakaolin in concentrated lime solutions. J Colloid Interface Sci. 2009;339(1):103–9.
38. Panagiotopoulou C, Kontori E, Perraki T, Kakali G. Dissolution of aluminosilicate minerals and by-products in alkaline media. J Mater Sci. 2007;42(9):2967–73.
39. Ambroise J, Maximilien S, Pera J. Properties of Metakaolin blended cements. Adv Cem Based Mater. 1994;1(4):161–8.
40. Taylor-Lange SC, Lamon EL, Riding KA, Juenger M. Calcined kaolinite-bentonite clay blends as supplementary cementitious materials. Appl Clay Sci. 2015;108:84–93.
41. Mermerdaş K, Gesoğlu M, Güneyisi E, Özturan T. Strength development of concretes incorporated with metakaolin and different types of calcined kaolins. Constr Build Mater. 2012;37:766–74.
42. Siddique R, Klaus J. Influence of metakaolin on the properties of mortar and concrete: A review. Appl Clay Sci. 2009;43(3–4):392–400.
43. Pustovgar E, Mishra RK, Palacios M, d'Espinose de Lacaillerie J-B, Matschei T, Andreev AS, et al. Influence of aluminates on the hydration kinetics of tricalcium silicate. Cem Concr Res. 2017;100:245–62.
44. Nicoleau L, Schreiner E, Nonat A. Ion-specific effects influencing the dissolution of tricalcium silicate. Cem Concr Res. 2014;59:118–38.
45. Begarin F, Garrault S, Nonat A, Nicoleau L. Hydration of alite containing aluminium. Adv Appl Ceram. 2011;110(3):127–30.
46. Bellmann F, Ludwig H-M. Analysis of aluminum concentrations in the pore solution during hydration of tricalcium silicate. Cem Concr Res. 2017;95:84–94.

47. Land G, Stephan D. Controlling cement hydration with nanoparticles. Cem Concr Compos. 2015;57:64–7.
48. Kumar A, Bishnoi S, Scrivener KL. Modelling early age hydration kinetics of alite. Cem Concr Res. 2012;42(7):903–18.
49. Kumar A, Oey T, Kim S, Thomas D, Badran S, Li J, et al. Simple methods to estimate the influence of limestone fillers on reaction and property evolution in cementitious materials. Cem Concr Compos. 2013;42:20–9.
50. Ley-Hernandez AM, Lapeyre J, Cook R, Kumar A, Feys D. Elucidating the effect of water-to-cement ratio on the hydration mechanisms of cement. ACS Omega. 2018;3(5):5092–105.
51. Bentz DP, Garboczi EJ, Haecker CJ, Jensen OM. Effects of cement particle size distribution on performance properties of Portland cement-based materials. Cem Concr Res. 1999;29(10):1663–71.
52. Givi AN, Rashid SA, Aziz F, Salleh M. Assessment of the effects of rice husk ash particle size on strength, water permeability and workability of binary blended concrete. Constr Build Mater. 2010;24(11):2145–50.
53. Justice JM, Kurtis KE. Influence of metakaolin surface area on properties of cement-based materials. J Mater Civ Eng. 2007;19(9):762–71.
54. Lagier F, Kurtis KE. Influence of Portland cement composition on early age reactions with metakaolin. Cem Concr Res. 2007;37(10):1411–7.
55. Al-Amoudi OS, Abduljauwad SN. Suggested modifications to ASTM standard methods when testing arid, saline soils. Geotech Test J. 1994;17(2):243–53.
56. Hamilton A, Hall C. A review of rehydroxylation in fired-clay ceramics. J Am Ceram Soc. 2012;95(9):2673–8.
57. Pignatelli I, Kumar A, Alizadeh R, Le Pape Y, Bauchy M, Sant G. A dissolution-precipitation mechanism is at the origin of concrete creep in moist environments. J Chem Phys. 2016;145(5):054701.
58. Erdogan ST, Quiroga PN, Fowler DW, Saleh HA, Livingston RA, Garboczi EJ, et al. Three-dimensional shape analysis of coarse aggregates: New techniques for and preliminary results on several different coarse aggregates and reference rocks. Cem Concr Res. 2006;36(9):1619–27.
59. Erdoğan ST, Nie X, Stutzman PE, Garboczi EJ. Micrometer-scale 3-D shape characterization of eight cements: particle shape and cement chemistry, and the effect of particle shape on laser diffraction particle size measurement. Cem Concr Res. 2010;40(5):731–9.
60. Holzer L, Flatt RJ, Erdoğan ST, Bullard JW, Garboczi EJ. Shape comparison between 0.4–2.0 and 20–60 μm cement particles. J Am Ceram Soc. 2010;93(6):1626–33.
61. Liu X, Garboczi EJ, Grigoriu M, Lu Y, Erdoğan ST. Spherical harmonic-based random fields based on real particle 3D data: improved numerical algorithm and quantitative comparison to real particles. Powder Technol. 2011;207(1):78–86.
62. Bullard JW, Garboczi EJ. A model investigation of the influence of particle shape on portland cement hydration. Cem Concr Res. 2006;36(6):1007–15.
63. Garboczi EJ, Bullard JW. Shape analysis of a reference cement. Cem Concr Res. 2004;34(10):1933–7.
64. Cook R, Ma H, Kumar A. Mechanism of tricalcium silicate hydration in the presence of polycarboxylate polymers. SN Appl Sci. 2019;1(2):145.
65. Taylor HF. Cement chemistry. London: Thomas Telford; 1997.
66. Oey T, Kumar A, Falzone G, Huang J, Kennison S, Bauchy M, et al. The influence of water activity on the hydration rate of tricalcium silicate. J Am Ceram Soc. 2016;99(7):2481–92.
67. Stoian J, Oey T, Bullard JW, Huang J, Kumar A, Balonis M, et al. New insights into the prehydration of cement and its mitigation. Cem Concr Res. 2015;70:94–103.
68. Zhang J, Scherer GW. Comparison of methods for arresting hydration of cement. Cem Concr Res. 2011;41(10):1024–36.
69. Scherer GW. Models of confined growth. Cem Concr Res. 2012;42(9):1252–60.
70. Scherer GW, Zhang J, Thomas JJ. Nucleation and growth models for hydration of cement. Cem Concr Res. 2012;42(7):982–93.
71. Bullard JW, Scherer GW, Thomas JJ. Time dependent driving forces and the kinetics of tricalcium silicate hydration. Cem Concr Res. 2015;74:26–34.
72. Bazzoni A, Ma S, Wang Q, Shen X, Cantoni M, Scrivener KL. The effect of magnesium and zinc ions on the hydration kinetics of C3S. J Am Ceram Soc. 2014;97(11):3684–93.
73. Scherer GW, Bellmann F. Kinetic analysis of CSH growth on calcite. Cem Concr Res. 2016;103:226–35.
74. Kumar A, Oey T, Falla GP, Henkensiefken R, Neithalath N, Sant G. A comparison of intergrinding and blending limestone on reaction and strength evolution in cementitious materials. Constr Build Mater. 2013;43:428–35.
75. Nelder JA, Mead R. A simplex method for function minimization. Comput J. 1965;7(4):308–13.
76. Bellmann F, Scherer GW. Analysis of CSH growth rates in supersaturated conditions. Cem Concr Res [Internet]. 2017; Available from: http://www.sciencedirect.com/science/article/pii/S0008884616301739.
77. Poon C-S, Lam L, Kou SC, Wong Y-L, Wong R. Rate of pozzolanic reaction of metakaolin in high-performance cement pastes. Cem Concr Res. 2001;31(9):1301–6.
78. Frıas M, De Rojas MS, Cabrera J. The effect that the pozzolanic reaction of metakaolin has on the heat evolution in metakaolin-cement mortars. Cem Concr Res. 2000;30(2):209–16.
79. Avet F, Scrivener K. Investigation of the calcined kaolinite content on the hydration of limestone calcined clay cement (LC3). Cem Concr Res. 2018;1(107):124–35.
80. Lasaga AC, Luttge A. Variation of crystal dissolution rate based on a dissolution stepwave model. Science. 2001;291(5512):2400–4.
81. Bentz DP, Ferraris CF, De la Varga I, Peltz MA, Winpigler JA. Mixture proportioning options for improving high volume fly ash concretes. Int J Pavement Res Technol. 2010;3(5):234.
82. de la Varga I, Castro J, Bentz DP, Zunino F, Weiss J. Evaluating the hydration of high volume fly ash mixtures using chemically inert fillers. Cem Concr Compos. 2017;161:221–8.
83. De Rojas MS, Luxan MP, Frías M, Garcia N. The influence of different additions on portland cement hydration heat. Cem Concr Res. 1993;23(1):46–54.
84. Brown PW, Franz E, Frohnsdorff G, Taylor H. Analyses of the aqueous phase during early C3S hydration. Cem Concr Res. 1984;14(2):257–62.
85. Bullard JW. A determination of hydration mechanisms for tricalcium silicate using a kinetic cellular automaton model. J Am Ceram Soc. 2008;91(7):2088–97.

How to cite this article: Lapeyre J, Ma H, Kumar A. Effect of particle size distribution of metakaolin on hydration kinetics of tricalcium silicate. *J Am Ceram Soc*. 2019;00:1–13. https://doi.org/10.1111/jace.16467